Allosteric Inhibition of Complement Function by a Staphylococcal Immune Evasion Protein

Supplementary Methods

This supplementary methods section features additional information to and extended versions of the methods provided in the main article. Citations either refer to the reference section of the main article or are listed at the end of this section (Supplementary References).

Protein Expression and Purification. Proteins were either isolated from human plasma (i.e. for C3 (39) and fB (40)) or recombinantly expressed and purified (i.e. for Efb-C and its RANA mutant (9), SCIN (5), fH(1-4) (25), Ba (7), and CRIg (24)) using established protocols. Compstatin (analog 4W9A; (Ac-ICVWQDWGAHRCT-NH_2) was produced using solid phase peptide synthesis as previously described (39). fH(19-20) was provided by Paul N. Barlow (University of Edinburgh, UK), and fH was purchased from Complement Technologies. C3b was generated by limited trypsinization of C3 and site-specifically biotinylated at the thioester sulfhydryl group using biotin-PEO-maleimide (Pierce) as described before (25).

Dynamic Conformation Analysis using Hydrogen-Deuterium Exchange Mass Spectrometry (HDX-MS). HDX-MS experiments were performed based on previously described protocols (16, 19, 21). On-exchange samples were prepared by mixing C3b with either Efb-C or RANA in PBS (12 mM phosphate, 138 mM NaCl, pH 7.4; DPBS; Gibco, Invitrogen) to final concentrations of 117 µM and 144 µM, respectively. After 10 min, the mixtures were diluted in deuterium PBS to a D_2O concentration of 50%. At various time points (10, 30, 100, 300, 1000, 3000, and 10000 s), each mixture was quenched using ice-cold 1 M TCEP, 7.4 M GuaHCl, pH 2.90 and kept on ice for 5 min to allow denaturation. All samples were diluted in 0.8% formic acid containing 16.6% glycerol and frozen at -80 ºC until analysis. Non-exchanged (incubation in PBS without D_2O) and equilibrium-exchanged samples (incubation in 0.5% formic acid in D_2O for two days at 23 ºC) were prepared as controls. Each sample was digested on a pepsin column (porcine pepsin coupled to 20AL Poros column; Perseptive Biosystems), separated using RP-HPLC (Vydac C18 HPLC column (1.0 mm, 5 µm, 50 mm), and analyzed by ESI-MS (Finnigan Classic LCQ MS; Thermo or Micromass electrospray Q-Tof MS; Waters). The analysis was performed at 0 ºC to minimize back-exchange and the raw data were acquired through Thermo SEQUEST or Waters Masslynx. Detected peptides were evaluated in DXMS explorer (Sierra Analytics Inc.) and the exchange level for each peptide was determined by dividing the incorporated deuteron number by the maximum deuteron number. HDX levels between active (C3b/Efb-C) and control samples (C3b/RANA) were compared and a difference of more than ±10% was considered significant.

Structural Analysis of C3b Complexes by Small Angle X-ray Scattering (SAXS). Prior to SAXS analysis, all samples were repurified by size exclusion chromatography (SEC) using an Ettan LC liquid chromatography system (GE Healthcare) configured with a 3-wavelength ultraviolet-visual (UV-VIS) detector. Purifications were performed on a Superdex 200 PC 3.2/2.4 ml column (GE Healthcare). C3b and C3b/Efb-C were purified in running buffer containing 20 mM Tris, 200 mM NaCl, pH 8.0 at 20 ºC. Flow-through fractions from each of the respective buffers were kept for buffer subtraction during SAXS analysis. SAXS data were collected at the ALS beamline 12.3.1 (SIBYLS) LBNL Berkeley, California (26). Wavelength λ=1.0 Å and the sample-to-detector distances set to 1.5 m resulting in scattering vectors, q, ranging from 0.01 $Å^{-1}$ to 0.32 $Å^{-1}$. The scattering vector is defined as $q = 4\pi \sin\theta/\lambda$, where 2θ is the scattering angle. All experiments were performed at 20°C and data was processed as described (26). Briefly, the data acquired at short and long time exposure (0.5s, 5s) were merged for calculations using the entire scattering spectrum. Concentration dependence was excluded by measuring at concentrations of 0.5 and 1.2 mg/ml, and the molecular weights were determined using a standard curve of reference proteins. Experimental SAXS data were investigated for aggregation using Guinier plots (30). The radius of gyration (R_G) was derived by Guinier approximation and GNOM (44) was used to compute pair-distance distribution functions, P(r), and the maximum macromolecule dimension D_{max}. In our BILBOMD strategy (31, 32), MD simulations were used to explore the conformational space adopted by CUB-TED. The MG core domains of C3b were treated as a single rigid body, while TED and CUB were considered as distinct rigid bodies connected by flexible linkers. Minimal ensemble search was used to identify the minimal ensemble of two conformers required to best fit the experimental data (31).

Allosteric Inhibition of Complement Function by a Staphylococcal Immune Evasion Protein

Supplementary Methods

Ligand binding assays using surface plasmon resonance. Binding studies were performed on a Biacore 2000 instrument (GE Healthcare) at 25 ºC using 10 mM HEPES pH 7.4, 150 mM NaCl, 1 mM $MgCl_2$, 0.005% Tween-20 as running buffer. Site-specifically biotinylated C3b was captured on streptavidin-coated sensor chips (SA chip or Biotin CAPture Kit; GE Healthcare), and 1 μM fB, Ba, fH (1-4), CRIg, SCIN, and compstatin were injected for 1 min each at a flow rate of 10 μl/min. The surface was regenerated with 1 M NaCl. A stable C3b/Efb-C complex was formed by injecting Efb-C (200 nM) into immobilized C3b for 1 min. The same panel of C3b ligands was injected to the C3b-Efb-C complex as described above and the SPR response (intensity, curve shape) was compared with binding to free C3b. After each injection to C3b/Efb-C, the surface was regenerated with 1 M NaCl and reconstituted with 20 nM Efb-C. The influence of Efb-C on convertase formation was monitored by injecting a 1:1 mixture of fB and fD (100 nM) on either immobilized C3b or the C3b/Efb-C complex for 2 min. After observing the regular convertase decay for 3 min, 1 μM fH was injected for 1 min to accelerate decay, and the surface was regenerated as described above. Data processing was performed using Scrubber (BioLogic Software Pty.) and included the subtraction of a reference flow cell (i.e. without C3b) and a set of buffer blank injections (double referencing; Ref. 45).

Atomic Coordinates and Structural Representations - Structural interpretations and modeling made use of the atomic coordinates found in the following PDB entries: C3b (2I07; Ref. 23), C3d/Efb-C (2GOX; Ref. 9), C3b/CRIg (2ICF; Ref. 24), C3c/Compstatin (2QKI; Ref. 32), CVF/fB (3HRZ; Ref. 14), C3b/fH(1-4) (2WII; Ref. 25), and $C3b_2Bb_2SCIN_2$ (2WIN; Ref. 7). In order to visualize the structural arrangement of the tested C3b ligands, all co-crystal structures were aligned with C3b via the stable MG ring domains (MG1-5) of C3b, C3c, and CVF, respectively. All structural images shown in the paper and supplementary appendix were rendered using an open-source version of PyMOL (www.pymol.org).

Supplementary References

44. Svergun D (1992) Determination of the regularization Parameter in Indirect-Transform Methods using perceptual criteria. *J Appl Cryst* 25:495-503.
45. Myszka DG, Improving biosensor analysis. J Mol Recognit 12:279-84.

Table S1

Table S1A: LIGPLOT contact list for CVF/Ba using PBD 3HRZ (14)

Ba (D*) residue	Ba (D*) atom	CVF (A,B,C) residue	CVF (A,B,C) atom	dist (Å)	Bond Type
Y110	CE2	L122	CD2	3.80	NNB
D108	OD2	R124	NH2	3.07	HHB
G109	C	F160	CZ	3.86	NNB
G109	CA	F160	CZ	3.81	NNB
G109	C	F160	CE1	3.83	NNB
G109	CA	F160	CE1	3.54	NNB
Y110	CZ	P163	CG	3.74	NNB
R80	CZ	I724	CG2	3.47	NNB
R92	NH2	D728	OD2	2.91	HHB
R92	NH1	D728	OD2	2.96	HHB
E88	CD	W733	CE3	3.76	NNB
E88	OE2	L734	N	2.83	HHB
D108	N	W735	O	2.95	HHB
D108	CB	W735	CD1	3.78	NNB
Y107	CA	L736	CD2	3.88	NNB
D108	CG	L736	C	3.85	NNB
D108	CG	L736	CA	3.82	NNB
D108	OD2	T737	OG1	2.47	HHB
P91	CB	Y757	CZ	3.31	NNB
P91	CA	Y757	CZ	3.88	NNB
P91	CB	Y757	CE2	3.40	NNB
P91	CA	Y757	CE2	3.53	NNB
W90	CZ2	Y757	CE2	3.63	NNB
W90	CE2	Y757	CE2	3.33	NNB
W90	CD2	Y757	CE2	3.79	NNB
W90	CD1	Y757	CE2	3.90	NNB
P91	CA	Y757	CD2	3.85	NNB
W90	CD1	Y757	CD2	3.71	NNB
R92	CB	Y757	CD1	3.85	NNB
R92	CD	Y757	CB	3.38	NNB
R92	CG	Y757	CB	3.61	NNB
R92	CB	Y757	CB	3.81	NNB
Y107	OH	R759	NH2	2.90	HHB
E88	OE1	R759	NE	3.26	HHB
R92	CZ	R759	CD	3.85	NNB
Q65	OE1	K840	NZ	2.98	HHB
R150	NE	D871	OD2	2.91	HHB
R150	NH2	D871	OD1	3.37	HHB
H165	NE2	D871	OD2	3.26	HHB
R157	NH1	E938	OE2	2.85	HHB
L158	CD2	R1262	CZ	3.50	NNB
L158	CD2	R1262	CD	3.84	NNB
E182	CD	R1262	CA	3.67	NNB
E182	OE2	E1263	N	2.53	HHB
D160	CA	K1284	CE	3.90	NNB
S53	CB	P1487	CB	3.78	NNB
S53	N	E1491	OE2	2.79	HHB

* corresponding residues 11-216 from fB (chain D)

Table S1B: LIGPLOT contact list for CVF/Bb using PDB 3HRZ (14)

Bb (D*) residue	Bb (D*) atom	CVF (A,B,C) residue	CVF (A,B,C) atom	dist (Å)	Bond Type
H367	O	T1496	OG1	2.76	HHB
N368	O	K1527	NZ	2.77	HHB
G370	N	Q1528	O	2.85	HHB
G371	CA	G1529	C	3.67	NNB
G370	C	G1529	C	3.89	NNB
D372	N	T1530	OG1	2.95	HHB
K325	NZ	E1615	O	3.12	HHB
T291	OG1	F1616	O	2.78	HHB
M369	CE	G1617	CA	3.57	NNB
M369	SD	G1617	CA	3.58	NNB
M369	CG	C1618	SG	3.76	NNB
N368	CG	C1618	SG	3.84	NNB
N368	CG	C1618	CB	3.64	NNB
G327	CA	C1618	C	3.79	NNB
S326	OG	P1619	O	2.70	HHB
S255	N	T1620	OXT	2.89	HHB
N368	ND2	T1620	O	2.89	HHB
T328	OG1	T1620	O	2.75	HHB
S253	CB	T1620	C	3.86	NNB
G254	CA	T1620	CA	3.89	NNB

* corresponding residues 236-739 from fB (chain D)

Table S1C: LIGPLOT contact list for C3c/Compstatin (4W9A) using PDB 2QKI (32)

4W9A (G) residue	4W9A (G) atom	C3c (A,B) residue	C3c (A,B) atom	dist (Å)	Bond Type
W4	N	G345	O	3.05	HHB
V3	CG2	M346	CE	3.88	NNB
V3	CG2	P347	CD	3.84	NNB
C2	N	N390	OD1	3.45	HHB
I1	N	N390	OD1	2.88	HHB
W4	CZ2	H392	CE1	3.71	NNB
W4	CB	P393	CG	3.59	NNB
V3	CG2	L454	CD2	3.79	NNB
V3	CG2	L454	CG	3.70	NNB
W7	CH2	L455	CD2	3.89	NNB
V3	CG1	R456	CD	3.46	NNB
V3	CG1	R456	CB	3.84	NNB
W7	NE1	M457	O	2.63	HHB
W7	CD1	R459	CA	3.70	NNB
W7	CZ2	E462	CB	3.66	NNB
W7	CE2	E462	CB	3.85	NNB
W7	CZ3	G489	C	3.56	NNB
G8	C	D491	CG	3.80	NNB
G8	CA	D491	CG	3.50	NNB
H10	CD2	D491	CB	3.86	NNB
Q5	NE2	D491	OD2	2.72	HHB
H10	N	D491	OD1	2.81	HHB

Additional Information for Tables S1A-G. All tables list the output data from binding site analyses performed using LIGPLOT (v4.5.3.; Ref. 40) and HBPLUS (v3.06; Ref. 41) showing the involved residue and atom pairs for each ligand and the corresponding complement fragment in the co-crystal as well as the distance between the atoms. The data sets for hydrogen bond (HHB) and hydrophobic interactions (NNB; cut-off 3.9 Å) have been combined. Brackets behind the ligand/ protein names contain the chain in the crystal structure. The lists have been sorted by increasing residue number in the C3 fragment or CVF.

Table S1 (continued)

Table S1D: LIGPLOT contact list for C3b/fH(1-4) using PDB 2WII (25)

FH1-4 (C) residue/atom		C3b (A,B) residue/atom		dist (Å)	Bond Type
R228	NH2	G42	O	3.09	HHB
E227	OE2	K43	NZ	3.07	HHB
E227	CG	K43	CD	3.67	NNB
E170	OE2	R72	NH1	2.61	HHB
E171	OE2	T140	OG1	3.06	HHB
E171	OE1	T140	OG1	2.91	HHB
A155	N	S157	O	2.80	HHB
G153	C	L158	CB	3.84	NNB
G153	O	S159	N	2.97	HHB
R157	NH2	E189	OE2	2.73	HHB
R157	NE	E189	OE2	3.25	HHB
R157	CZ	E189	CD	3.84	NNB
N84	CB	Q558	CD	3.84	NNB
N60	NH2	D732	OD1	2.78	HHB
L41	O	I733	N	3.09	HHB
R39	CZ	I734	CD1	3.83	NNB
R65	NH2	E737	O	2.83	HHB
R39	NH2	N738	O	2.80	HHB
G68	CA	V740	CG1	3.48	NNB
H69	CG	E744	CG	3.61	NNB
H69	CB	E744	CG	3.44	NNB
L80	CD2	F772	CZ	3.59	NNB
L80	CB	F772	CZ	3.69	NNB
L80	CD2	F772	CE1	3.85	NNB
F86	CZ	F772	CD1	3.44	NNB
F86	CZ	F772	CG	3.68	NNB
D72	OD2	K774	NZ	2.74	HHB
L41	CD1	H897	C	3.48	NNB
R39	CD	F898	CZ	3.30	NNB
S40	CA	F898	CE1	3.75	NNB
L41	CD2	F898	CD1	3.44	NNB
L41	CG	F898	CD1	3.86	NNB
R39	NH2	S900	OG	2.98	HHB
R214	NH1	N1069	OD1	2.79	HHB
R228	CD	N1069	C	3.74	NNB
Q216	NE2	S1075	OG	2.82	HHB
Q216	CD	I1135	CG2	3.88	NNB
R214	CD	I1135	CG1	3.65	NNB
Q205	N	E1138	OE2	3.25	HHB
S204	CB	E1138	CD	3.51	NNB
M144	CE	S1293	CB	3.42	NNB

Table S1E: LIGPLOT contact list for C3b/CRIg using PDB 2ICF (24)

CRIg (S) residue/atom		C3b (A,B) residue/atom		dist (Å)	Bond Type
D87	CG	I213	CG2	3.62	NNB
D87	CG	T234	CB	3.87	NNB
E85	OE2	K242	NZ	2.89	HHB
V107	CG1	R444	CZ	3.86	NNB
V107	CG1	R444	CD	3.80	NNB
V107	CB	R444	CD	3.66	NNB
L50	CD2	K544	CE	3.64	NNB
H57	CD2	K544	CD	3.71	NNB
H57	CG	K544	CD	3.87	NNB
D52	OD2	K544	NZ	2.75	HHB
T47	OG1	D797	OD2	3.19	HHB
Q60	CD	E800	CD	3.84	NNB
Q60	CB	E800	CD	3.85	NNB
Q60	CA	E800	CD	3.85	NNB
A61	N	E800	OE1	3.04	HHB
Q59	O	E800	N	3.00	HHB

Table S1F: LIGPLOT contact list for C3b/SCIN (site 1) using PDB 2WIN (7)

SCIN (N) residue/atom		C3b (A,B) residue/atom		dist (Å)	Bond Type
R42	NH1	P555	O	3.22	HHB
Y39	CD1	G556	C	3.62	NNB
Y39	CG	G556	C	3.63	NNB
Y39	CB	G556	C	3.65	NNB
Y39	CB	G556	CA	3.88	NNB
Y40	OH	Q558	OE1	2.92	HHB
K56	NZ	D730	OD1	2.63	HHB
Y53	CZ	D732	CG	3.57	NNB
Y53	CE2	D732	CG	3.60	NNB
Y53	CZ	D732	CB	3.73	NNB
R42	CB	V740	CB	3.65	NNB
Y53	CD2	F898	CZ	3.65	NNB
Y53	CG	F898	CZ	3.67	NNB
Y53	CB	F898	CZ	3.60	NNB
K50	CA	F898	CE2	3.90	NNB
K50	CG	F898	CD1	3.66	NNB
K50	CG	F898	CG	3.76	NNB
K50	CB	F898	CG	3.82	NNB
K50	CD	F898	CB	3.81	NNB

* corresponds to one of two SCIN-A molecules in the complex of the SCIN-stabilized C3 convertase dimer ($C3b_2Bb_2SCIN_2$). Both SCIN have contact residues on separate sites of the same C3b.

Table S1G: LIGPLOT contact list for C3b/SCIN (site 2) using PDB 2WIN (7)

SCIN (Q) residue/atom		C3b (A,B) residue/atom		dist (Å)	Bond Type
Y68	CB	N835	CB	3.53	NNB
K61	O	Q836	NE2	3.12	HHB
S64	OG	E837	N	3.22	HHB
S64	CB	E837	CG	3.49	NNB
N8	OD1	K839	NZ	3.03	HHB
F60	CE1	K839	CE	3.46	NNB
F60	CD1	K839	CE	3.29	NNB
F60	CG	K839	CE	3.85	NNB
F60	CE2	K839	CB	3.83	NNB
F60	CD2	K839	CB	3.87	NNB
F60	CZ	T865	CG2	3.63	NNB
Q11	CG	T865	CB	3.87	NNB
Y68	CZ	P868	CD	3.54	NNB
Y68	CZ	P868	CG	3.42	NNB
Y68	CE2	P868	CG	3.64	NNB
D59	CG	H896	CE1	3.83	NNB
K61	CD	H896	CB	3.53	NNB
K61	CB	H896	CB	3.87	NNB
K14	CE	S1417	CB	3.75	NNB
K14	CD	S1417	CB	3.49	NNB
L4	CD1	Q1443	CD	3.54	NNB
Y10	CE1	Y1444	CD1	3.58	NNB
Y10	CD1	Y1444	CD1	3.54	NNB
Y10	CE1	Y1444	CB	3.49	NNB
S7	C	F1445	CZ	3.59	NNB
S7	CA	F1445	CZ	3.27	NNB
T6	C	F1445	CZ	3.75	NNB
S7	CA	F1445	CE2	3.68	NNB
Q11	CD	F1445	CE1	3.85	NNB
Y10	CB	F1445	CE1	3.85	NNB
L4	CD1	N1446	CB	3.44	NNB
L4	CB	N1446	CB	3.26	NNB

* see footnote in Table S1F

Figure S1

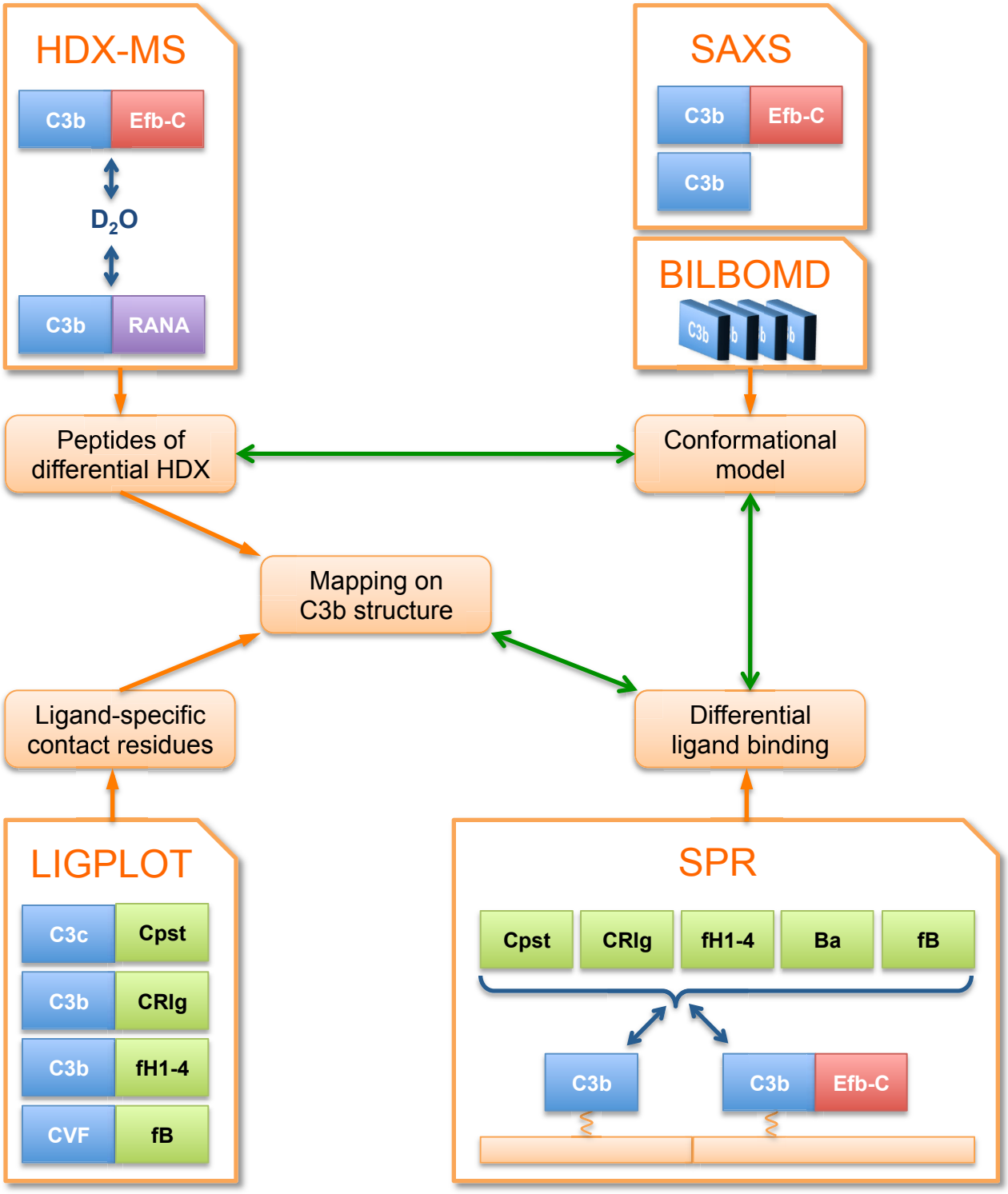

Figure S1. Schematic representation of the experimental setup of the study. Various methods were used in this study for exploring the effect of Efb-C on the structure (HDX-MS, SAXS, BILBOMD) and function (SPR) of C3b. Together with binding site analysis of available co-crystal structures (LIGPLOT), the individual results were compared for cross-validation (green arrows) and were used to build a structural model of the allosteric effects induced by Efb-C.

Allosteric Inhibition of Complement Function by a Staphylococcal Immune Evasion Protein

Figure S2

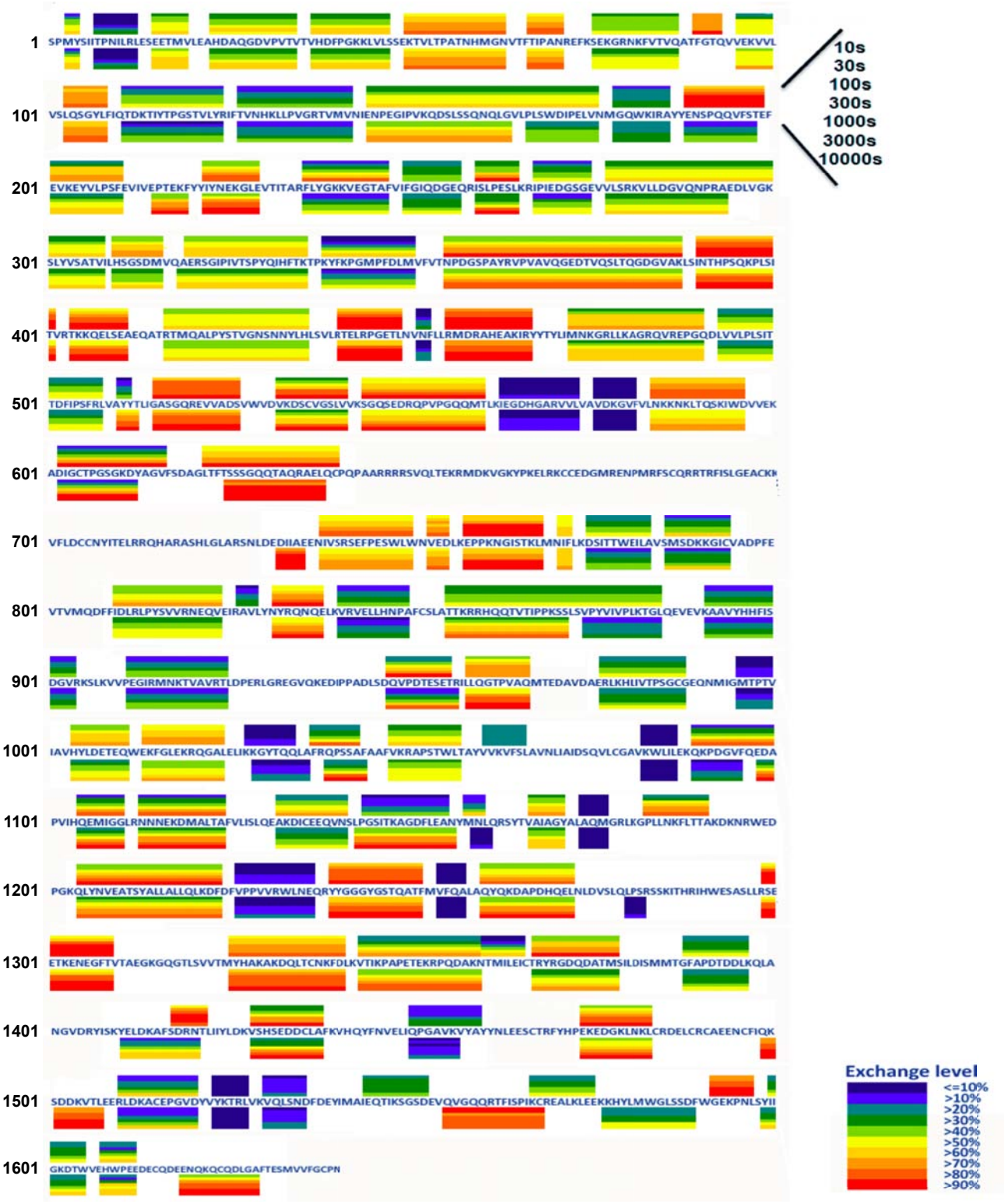

Figure S2. Detailed H/D exchange map for C3b in the presence of Efb-C or RANA. Aligned with the primary sequence of C3, the two sets of *colored bars* represent H/D exchange for C3b/RANA (upper set) and C3b/Efb-C (lower set). Each set is divided into rows corresponding to different exchange time points (10s, 30s, 100s, 300s, 1000s, 3000s and 10000s; *top* to *bottom*). The *color coding* indicates the percentage of H/D exchange at the given time point (see legend).

Allosteric Inhibition of Complement Function by a Staphylococcal Immune Evasion Protein

Figure S3

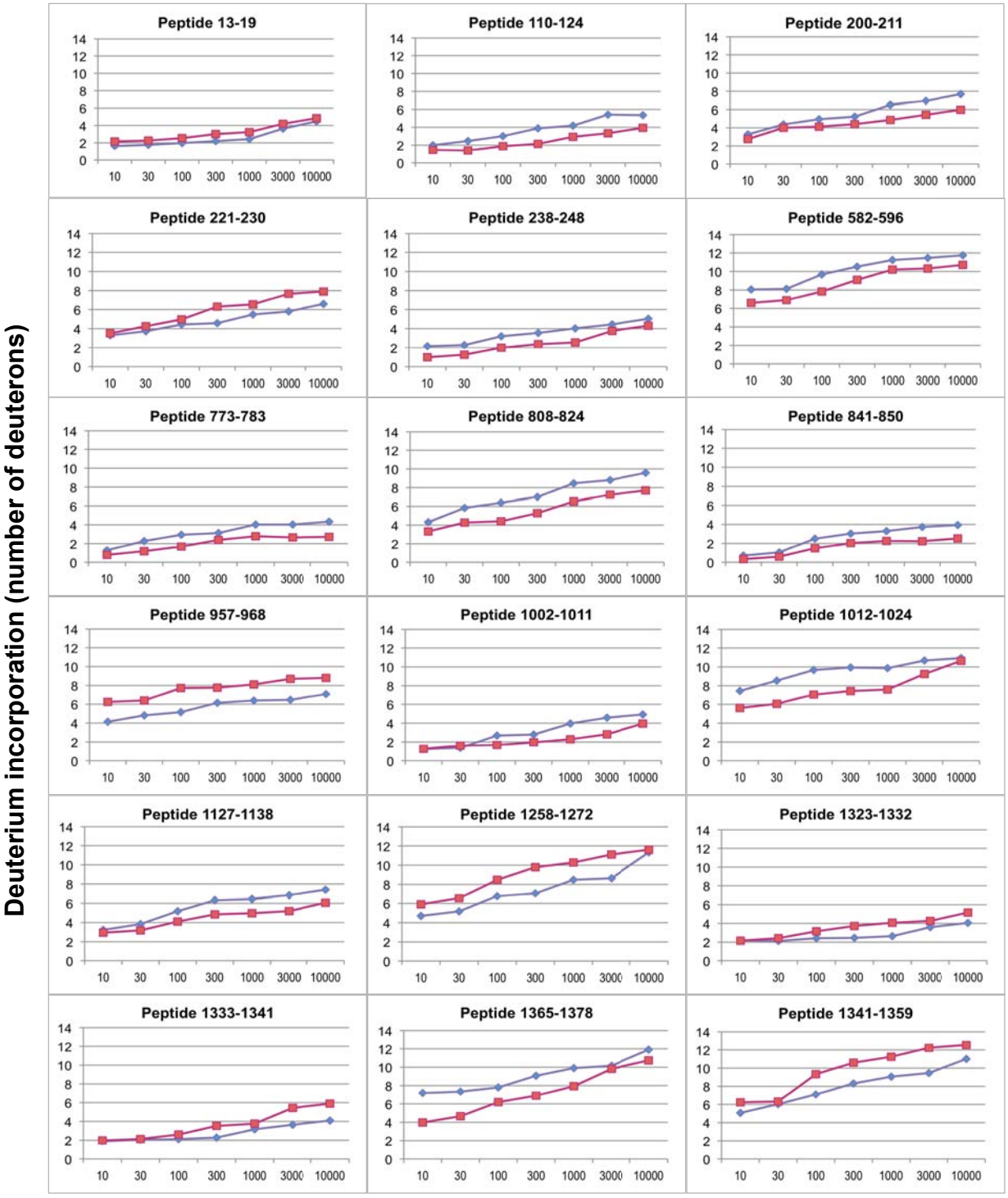

Figure S3. Time-resolved increase of deuterium content. The absolute number of deuterium for each segment of C3b bearing significant difference in exchange level after binding of Efb-C is shown for all seven time points (10-10,000 s). The number on top of each panel specifies the residue range of the peptide segment. Blue dots indicate HDX experiments with C3b/RANA while red squares indicate those with C3b/Efb-C. The X-axis represents the H/D exchange time in seconds and the Y-axis indicates the number of exchanged deuterium.

Figure S4

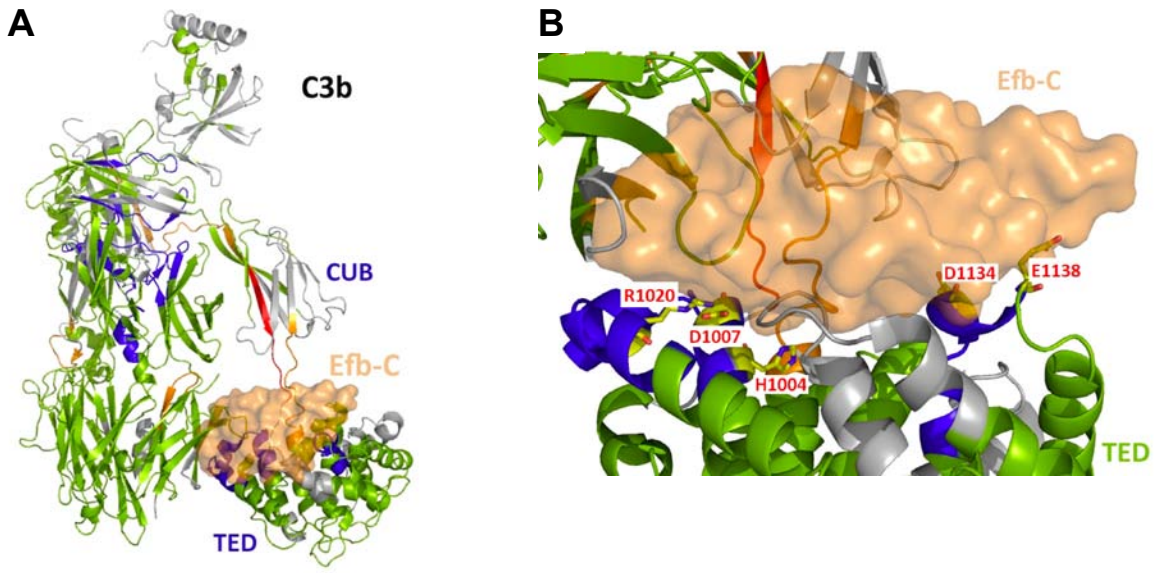

Figure S4. H/D exchange at the proposed interaction site of Efb-C on C3b. (**A)** Based on the C3d/Efb-C co-crystal structure (PDB 2GOX) (9), Efb-C was aligned to the C3b structure (PDB 2I07) (23). According to the deuterium exchange results, two peptide segments in TED domain (1002-1011 and 1012-1024) showed decreased exchange level in C3b/Efb-C complex. In these two segments, five of seven residues that were previously determined to be key residues within the C3d/Efb-C interaction site were covered (**B**) indicating that Efb-C is bound to C3b at the similar even same sites as where it is bound to C3d. As binding of Efb-C to this site on the TED domain of C3b would cause a steric clash with the MG ring of C3b in this arrangement, this further supports the necessity of structural rearrangements.

Figure S5

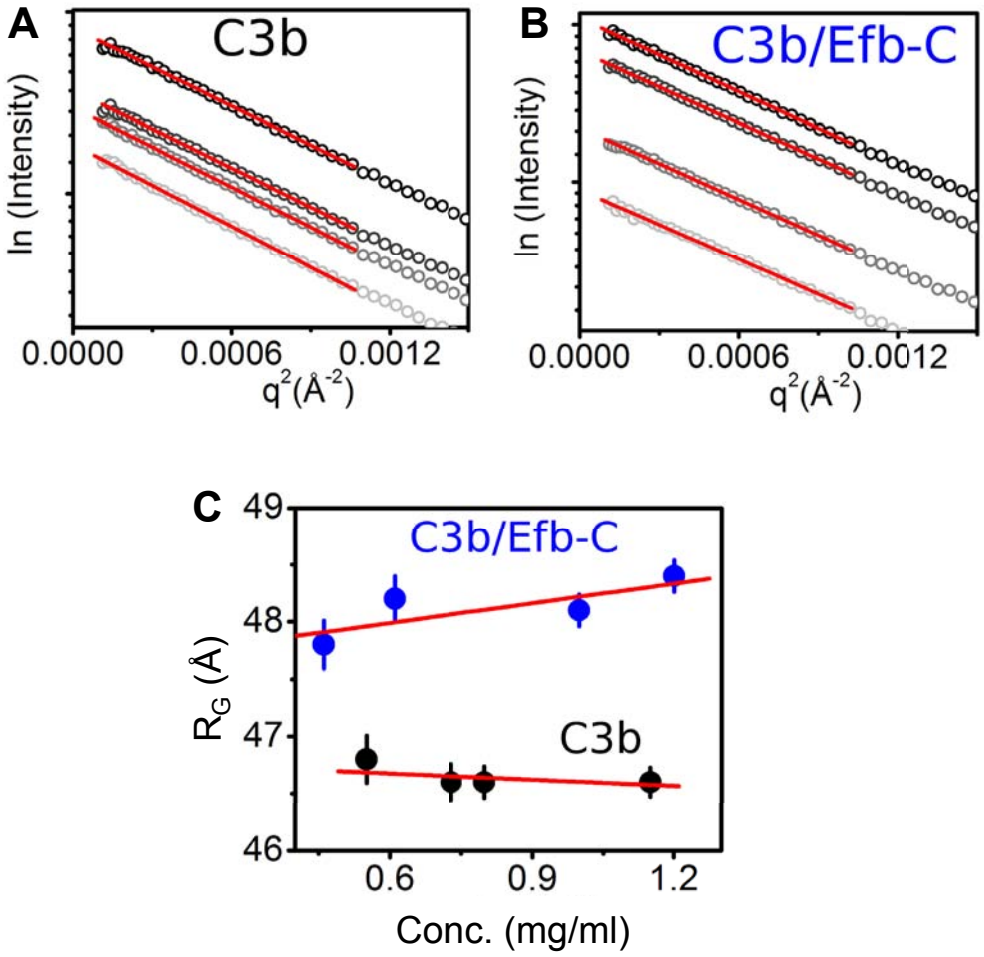

Figure S5. Additional data of the SAXS analysis of C3b and C3b/Efb-C. (**A, B**) Experimental X-ray Guinier R_G of free C3b (**A**) and the C3b/Efb-C complex (**B**). The q ranges used for the R_G fits were 0.011 to 0.1 $Å^{-1}$ for C3b, and 0.011 to 0.099 $Å^{-1}$ for C3b/Efb-C. (**C**) Concentration dependence of the Guinier R_G for free C3b (blue) and C3b/Efb-C (black).

Figure S6

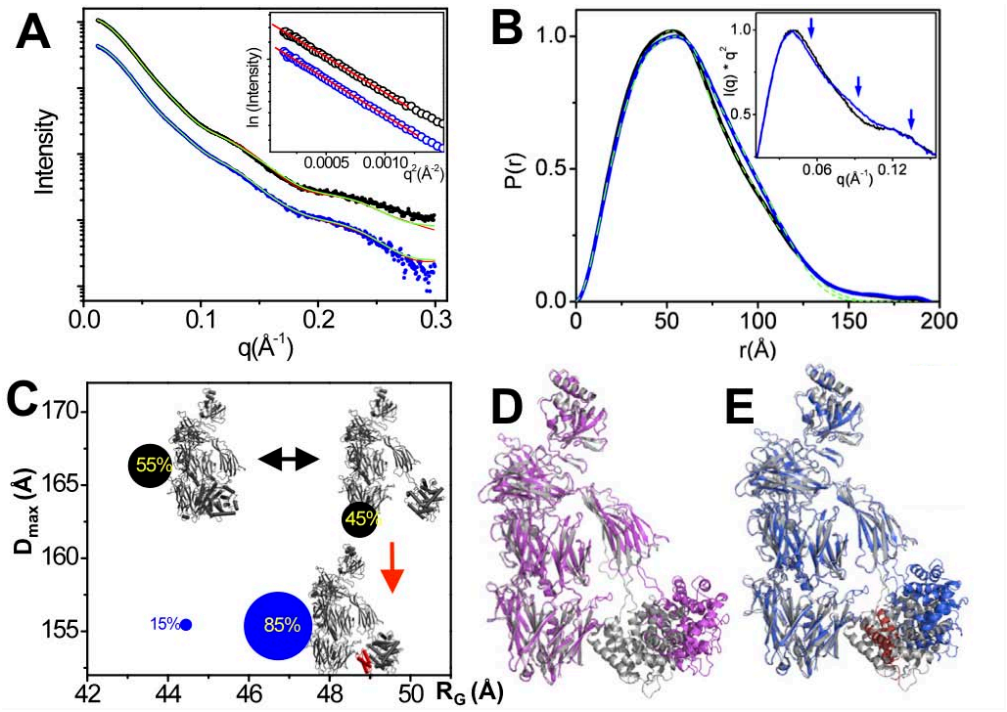

Figure S6. SAXS analysis of C3b and C3b/Efb-C in buffer containing 5% glycerol. (**A**) Experimental scattering curves with Guinier plots (insert) and (**B**) pair distribution function for C3b (black) and C3b/Efb-C (blue). (**C**) R_G/D_{max} plot showing volume ratios of free C3b (black) and C3b/Efb-C alongside with rigid body modeling-derived conformers. (**D, E**) Superposition of the models for C3b (magenta; **D**) and C3b/Efb-C (blue/red; **E**) with the crystal structure of C3b (PDB 2I07; Ref. 23; grey).

Figure S7

A

```
3HRZ:   2   LYTLITPAVLRTDTEEQILVEAHGDSTPKQLDIFVHDFPRKQKTLFQTRVDMNPAGGMLV  61
2I07:   3   MYSIITPNILRLESEETMVLEAHDAQGDVPVTVTVHDFPGKKLVLSSEKTVLTPATNHMG  62

3HRZ:  62   TPTIEIPA-KEVSTDSRQNQYVVVQVT-GPQVRLEKVVLLSYQSSFLFIQTDKGIYTPGS  119
2I07:  63   NVTFTIPANREFKSEKGRNKFVTVQATFGTQV-VEKVVLVSLQSGYLFIQTDKTIYTPGS  121

3HRZ: 120   PVLYRVFSMDHNTSKMNKTVIVEFQTPEGILVSSNSVD-------LNFFWTYNLPDLVSL  172
2I07: 122   TVLYRIFTVNHKLLPVGRTVMVNIENPEGIPVKQDSLSSQNQLGVLPLSW--DIPELVNM  179

3HRZ: 173   GTWRIVAKYEHSPEN-YTAYFDVRKYVLPSFEVRLQPSEKFFYIDGNENFHVSITARYLY  231
2I07: 180   GQWKIRAYYENSPQQVFSTEFEVKEYVLPSFEVIVEPTEKFYYIYNEKGLEVTITARFLY  239

3HRZ: 232   GEEVEGVAFVLFGVKIDDAKKSIPDSLTRIPIIDGDGKATLKRDTFRSRFPNLN--ELVG  289
2I07: 240   GKKVEGTAFVIFGIQDGEQRISLPESLKRIPIEDGSGEVVLSRKVLLDGVQNLRAEDLVG  299

3HRZ: 290   HTLYASVTVMTESGSDMVVTEQSGIHIVASPYQIHFTKTPKYFKPGMPYELTVYVTNPDG  349
2I07: 300   KSLYVSATVILHSGSDMVQAERSGIPIVTSPYQIHFTKTPKYFKPGMPFDLMVFVTNPDG  359

3HRZ: 350   SPAAHVPVVSEAFHSMGT-TLSDGTAKLILNIPLNAQSLPITVRTNHGDLPRERQATKSM  408
2I07: 360   SPAYRVPVAVQGEDTVQSLTQGDGVAKLSINTHPSQKPLSITVRTKKQELSEAEQATRTM  419

3HRZ: 409   TAIAYQTQGGSGNYLHVAITSTEIKPGDNLPVNFNVKGNANSLKQIKYFTYLILNKGKIF  468
2I07: 420   QALPYSTVGNSNNYLHLSVLRTELRPGETLNVNFLLRMDRAHEAKIRYYTYLIMNKGRLL  479

3HRZ: 469   KVGRQPRRDGQNLVTMNLHITPDLIPSFRFVAYYQV----GNNEIVADSVWVDVKDTCMG  524
2I07: 480   KAGRQVREPGQDLVVLPLSITTDFIPSFRLVAYYTLIGASGQREVVADSVWVDVKDSCVG  539

3HRZ: 525   TLVVK---GDNLIQMPGAAMKIKLEGDPGARVGLVAVDKAVYVLNDKYKISQAKIWDTIE  581
2I07: 540   SLVVKSGQSEDRQPVPGQQMTLKIEGDHGARVVLVAVDKGVFVLNKKNKLTQSKIWDVVE  599

3HRZ: 582   KSDFGCTAGSGQNNLGVFEDAGLALTTSTNLNTKQRSAAKCPQPA  626
2I07: 600   KADIGCTPGSGKDYAGVFSDAGLTFTSSSGQQTAQRAELQCPQPA  644

3HRZ: 714    EDGFIADSDITSRSLFPKSWLWLTKDLTEEPNSQGISSKTMSFYLRDSITTWVVLAVSFT  773
2I07: 730    DEDIIAEENIVSRSEFPESWLWNVEDLKEPPKN-GISTKLMNIFLKDSITTWEILAVSMS  788

3HRZ: 774    PTKGICVAEPYEIRVMKVFFIDLQMPYSVVKNEQVEIRAILHNY-VNEDIYVRVELLYNP  832
2I07: 789    DKKGICVADPFEVTVMQDFFIDLRLPYSVVRNEQVEIRAVLYNYRQNQELKVRVELLHNP  848

3HRZ: 833    AFCSASTKGQRYRQQFPIKALSSRAVPFVIVPLEQGLHTVEIKASVQEALWSDGVRKKLK  892
2I07: 849    AFCSLATTKRRHQQTVTIPPKSSLSVPYVIVPLKTGLQEVEVKAAVYHHFISDGVRKSLK  908

3HRZ: 893    VVPEGVQ-KSIVTIVKLDPRAKGVGGTQLEVIKARKLDDRVPDTEIETKIIIQGDPVAQI  951
2I07: 909    VVPEGIRMNKTVAVRTLDPERLGREGVQKEDIPPADLSDQVPDTESETRILLQGTPVAQM  968

3HRZ: 952    IENSIDGSKL  961
2I07: 969    TEDAVDAERL  978

3HRZ: 1246  PTHKDLNLDITIELPDREVPIRYRINYENALLARTVETKLNQDITVTASGDGKATMTILT  1305
2I07: 1265  PDHQELNLDVSLQLPSRSSKITHRIHWESASLLRSEETKENEGFTVTAEGKGQGTLSVVT  1324

3HRZ: 1306  FYNAQLQEKANVCNKFHLNVSVE---NIHLNAMGAKGALMLKICTRYLGEVDSTMTIIDI  1362
2I07: 1325  MYHAKAKDQLT-CNKFDLKVTIKPAPETEKRPQDAKNTMILEICTRYRGDQDATMSILDI  1383

3HRZ: 1363  SMLTGFLPDAEDLTRLSKGVDRYISRYEVDNNMAQKVAVIIYLNKVSHSEDECLHFKILK  1422
2I07: 1384  SMMTGFAPDTDDLKQLANGVDRYISKYELDKAFSDRNTLIIYLDKVSHSEDDCLAFKVHQ  1443

3HRZ: 1423  HFEVGFIQPGSVKVYSYYNLDEKCTKFYHPDKGTGLLNKICIGNVCRCAGETCSSLNHQE  1482
2I07: 1444  YFNVELIQPGAVKVYAYYNLEESCTRFYHPEKEDGKLNKLCRDELCRCAEENCFIQKSDD  1503

3HRZ: 1483  RIDVILQIEKACETNVDYVYKTKLLRIEEQDGNDIYVMDVLEVIKQGTDENPRAKTHQYI  1542
2I07: 1504  KVTLTERLDKACEPGVDYVYKTRLVKVQLSNDFDEYIMAIEQTIKSGSDEVQVGQQRTFI  1563

3HRZ: 1543  SQRKCQEALNLKVNDDYLIWGSRSDLLPTKDKISYIITKNTWIERWPHEDECQEEEFQKL  1602
2I07: 1564  SPIKCREALKLEEKKHYLMWGLSSDFWGEKPNLSYIIGKDTWVEHWPEEDECQDEENQKQ  1623

3HRZ: 1603  CDDFAQFSYTLTEFGCPT  1620
2I07: 1624  CQDLGAFTESMVVFGCPN  1641
```

B

CVF	C3b
L122	L124
R124	R126
F160	L169
P163	-
I724	V740
D728	E744
W733	W749
L734	L750
W735	W751
L736	N752
T737	V753
Y757	F772
R759	K774
K840	T856
D871	E887
E938	E955
R1262	R1281
E1263	S1282
K1284	K1303
P1487	E1508
E1491	D1512
T1496	P1517
K1527	K1548
Q1528	S1549
G1529	G1550
T1530	S1551
E1615	V1636
F1616	F1637
G1617	G1638
C1618	C1639
P1619	P1640
T1620	N1641

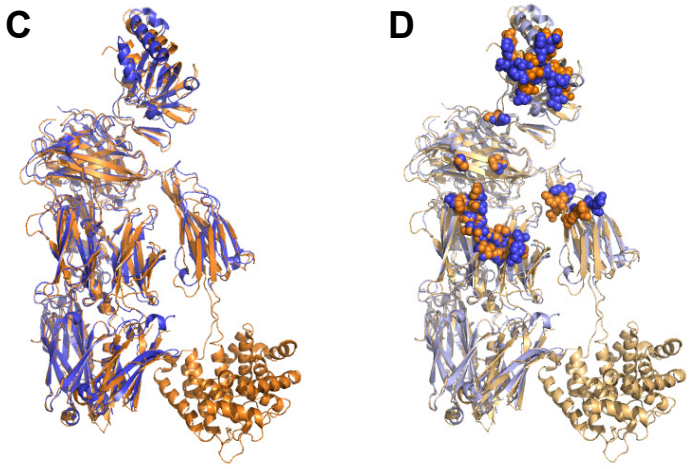

Figure S7. Mapping of fB binding sites on CVF and C3b. (A) Sequence alignment of CVF (PDB 3HRZ; chains A-C) (14) and C3b (PDB 2I07 chains A-B) (23) with LigPLOT contact residues for segments Ba and Bb (**Table S1A,B**) marked in red and green, respectively. **(B)** List of contact residues for Ba (red) and Bb (green) in CVF and C3b. **(C-D)** Structure overlay of CVF (blue) and C3b (orange) in cartoon representation (**C**) and with contact residues shown as spheres (**D**).

Figure S8

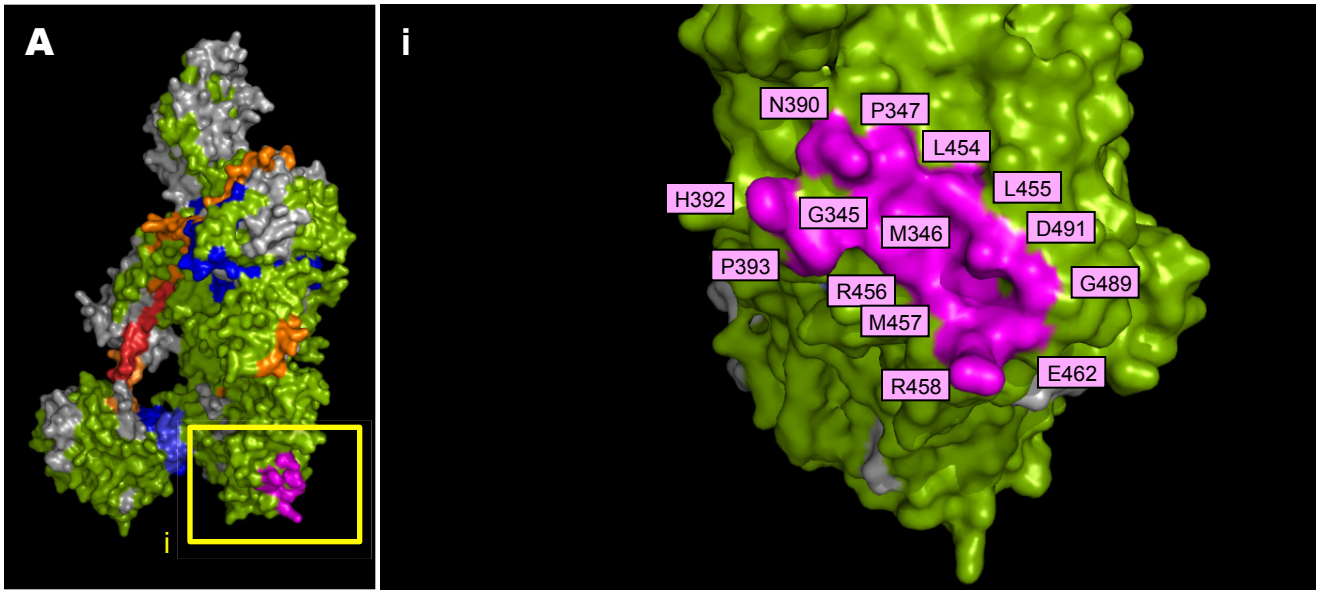

Figure S8A. Detailed binding site analysis for Compstatin on C3b. No peptides of significantly altered HDX could be found near the contact site for compstatin between domains MG4 and MG5.

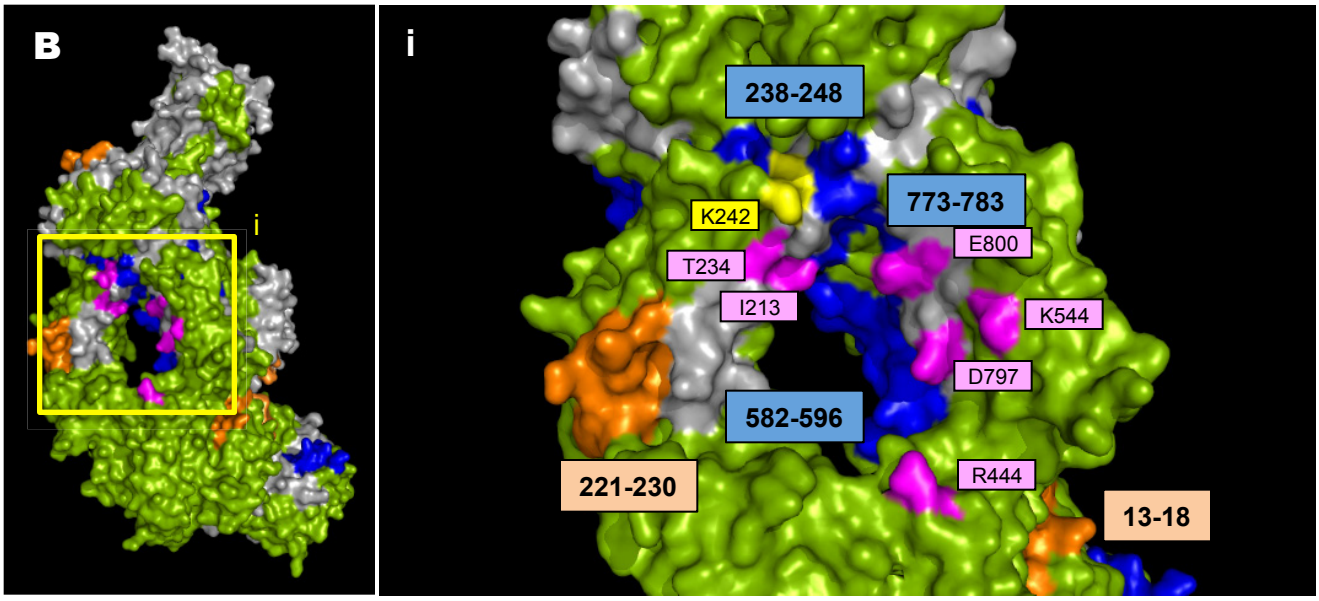

Figure S8B. Detailed binding site analysis for CRIg on C3b. In case of the CRIg contact site, four residues (T234, R444, K544, D797) are clearly distant from any peptides that experienced changes in HDX. Another two (I213, E800) lie nearby more protected peptides (200-211 and 773-782, respectively). A single residue (K242, yellow) is located in the middle of a rather large peptide, that may become more protected due to its surrounding domains (see **Fig. S9**).

Additional Information for Fig. S8A-F. All contact residues for individual ligands (magenta) were derived from the LIGPLOT analysis (**Table S1A-G**) and mapped on the crystal structure of C3b (PDB 2I07) (27) together with peptides that experienced significant (>20% = red, >10% = orange, <-10% = blue) or no significant changes (less than ±10% = green). Areas not detected by HDX-MS are shown in grey. Residues that are part of both a contact site and a peptide of significant change are highlighted in yellow.

Figure S8 (continued)

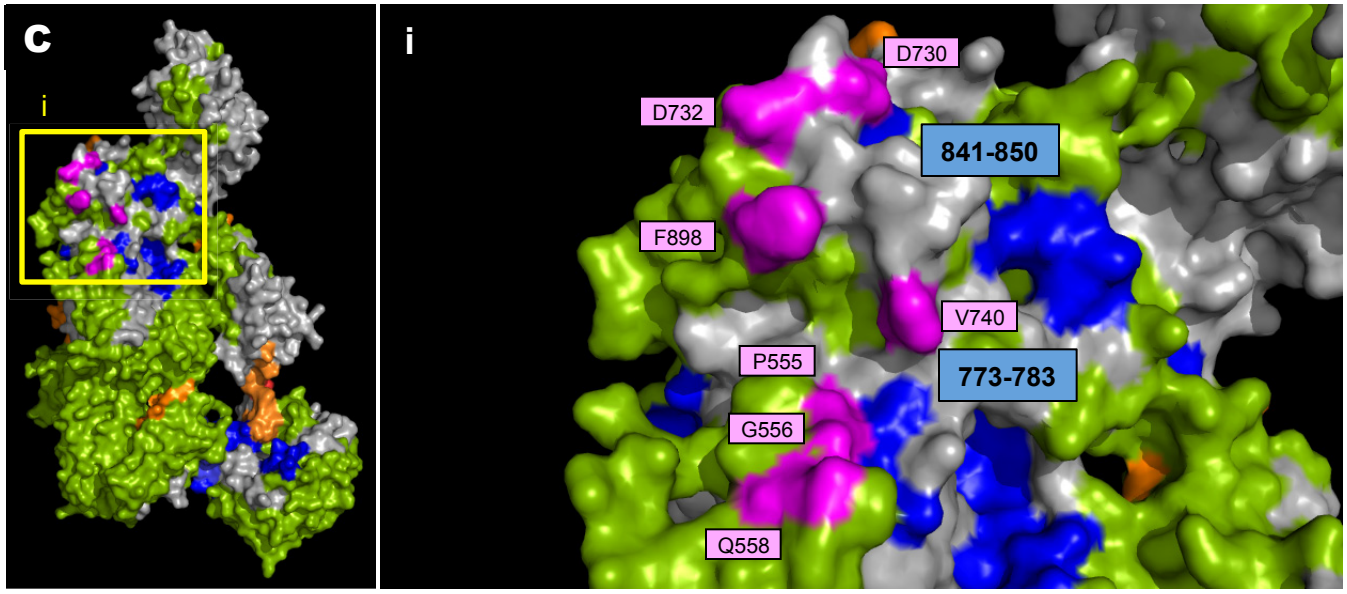

Figure S8C. Detailed binding site analysis for SCIN (site 1) on C3b. The majority of the contact residues within this site are clearly distant to peptides that experiences significant HDX. The three residues (P555, G556, D730) in direct neighborhood to changed peptides (773-783, 841-850) are all part of different segments. In both cases, the involved residues are located at the N-terminus (L773-D775, R841) of rather large peptides (11 and 10 amino acids, respectively).

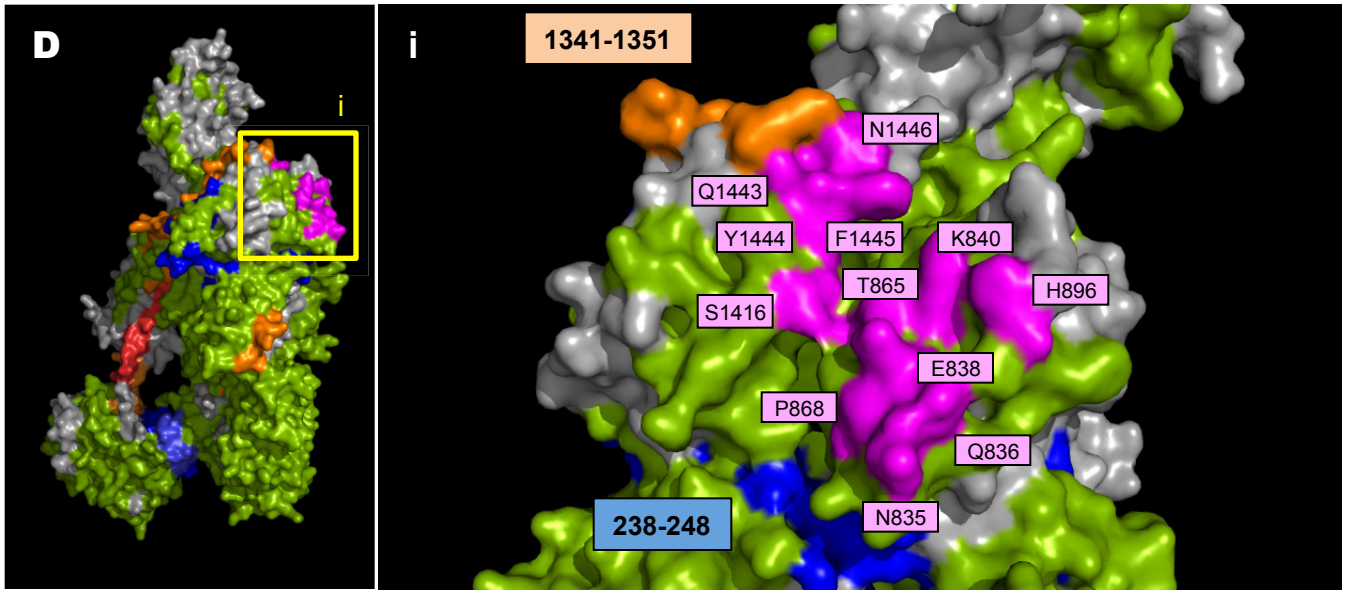

Figure S8D. Detailed binding site analysis for SCIN (site 2) on C3b. The second site for SCIN covers domains MG7 and MG8. Though it appears near the SCIN site in the close-up figure, peptide 238-348 is located clearly distant on MG3. Peptide 1341-1349 is the only peptide that is close to the site with residues Q1443 and N1446 being adjacent to K1351. However, since two peptides extending on the N-terminal side also experienced substantial HD exposure (i.e. 1323-1332 and 1333-1341), it is likely that the major changes occur on the N-terminal part of peptide 1341-1351.

Figure S8 (continued)

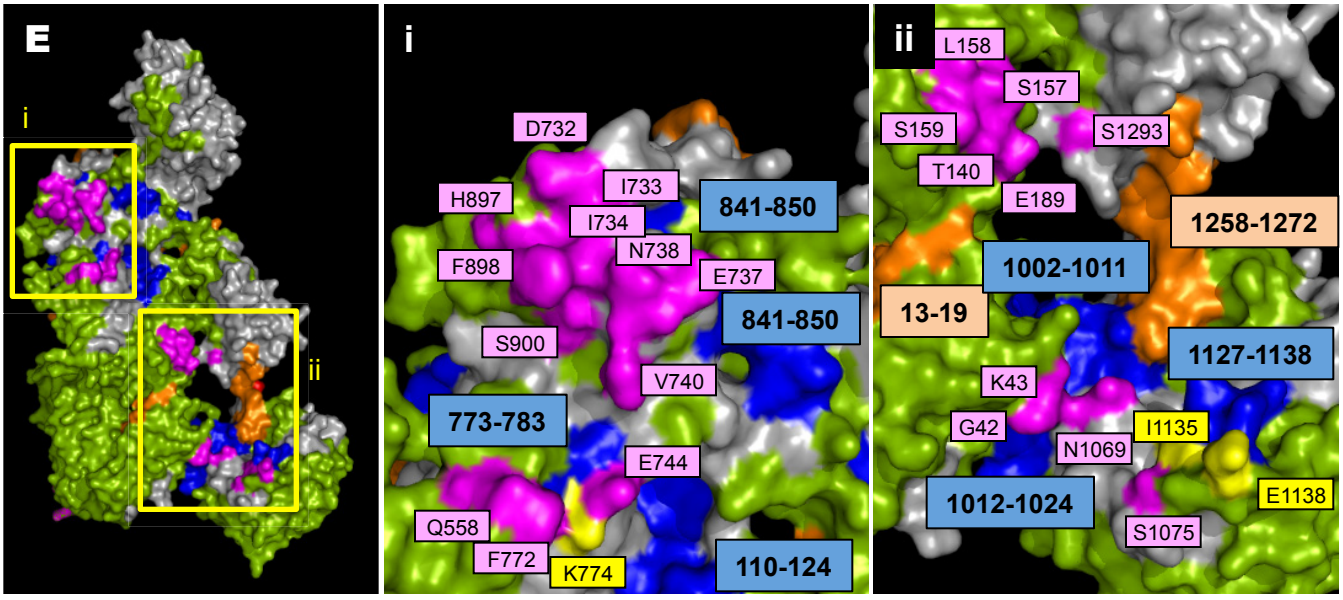

Figure S8E. Detailed binding site analysis for fH(1-4) on C3b. Among the distributed binding patches for fH(1-4), there are three residues (K774, I1135, E1138) that are part of peptides that experienced decreased HDX after binding of Efb-C (i.e. 773-783 and 1127-1138). The latter two residues are near the Efb-C site on TED and may be influenced by direct shielding (**Fig. S10**). Another residue (F772) is immediately adjacent (773-783) and several others in close neighborhood to affected peptides (i.e. G42 to 1012-1024, I734 to 841-850, E744/F772 to 773-783, and S1075 to 1127-1138).

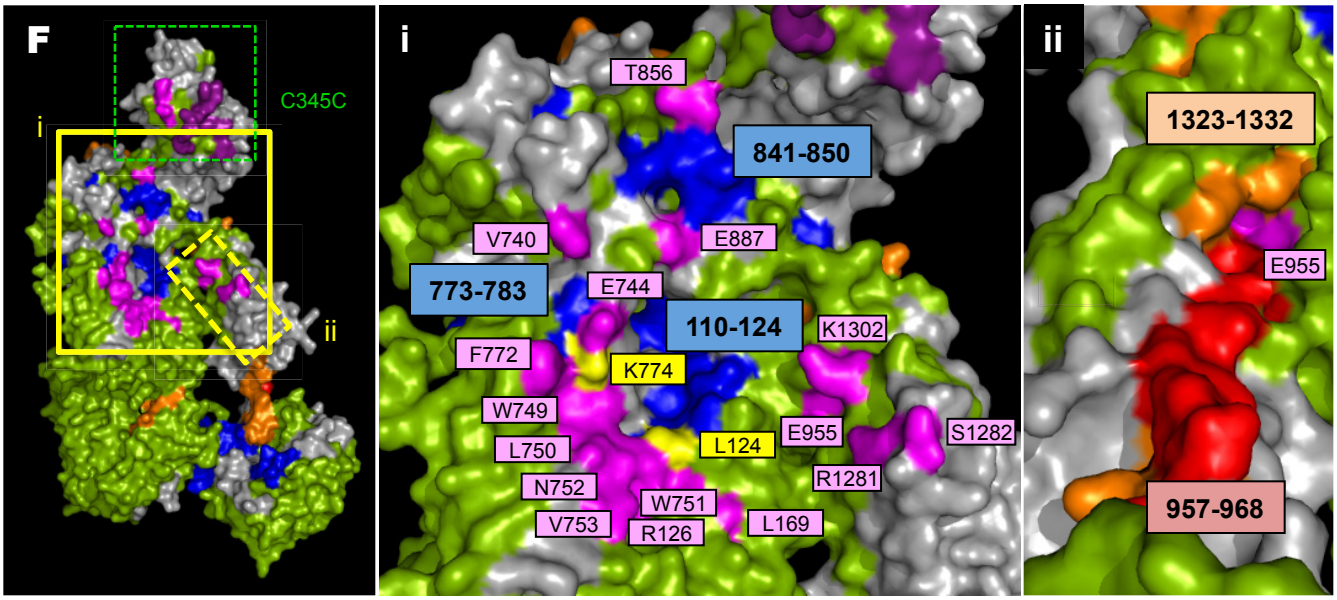

Figure S8F. Detailed binding site analysis for fB on C3b. As in the case of segment Ba (magenta), K774 is within and E744/F772 nearby a peptide that experienced HDX protection upon Efb-C binding (773-783). In addition, L124 is part of a protected peptide (110-124) and E995 is situated between two peptides of strong exposure (957-968 and 1323-1332). Finally, W749, W751, T856, E887 are also in close neighborhood to areas of change. No altered peptides were detected for segments Ba and Bb (dark purple) in the C345C region of C3b. Contact residues were derived from analysis of CVF-fB and transferred to the corresponding residues on C3b via sequence alignment (**Fig. S7**)

Figure S9

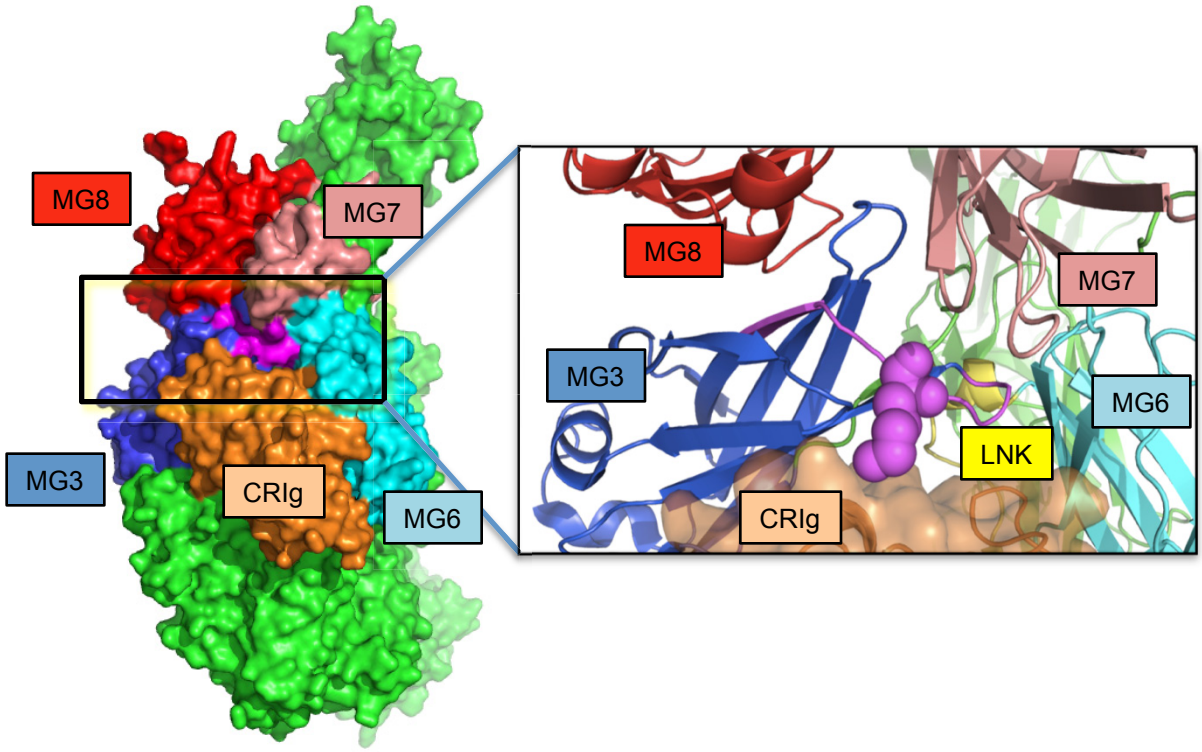

Figure S9. Potential influence of surrounding domains on solvent exposure of a peptide containing a CRIg contact residue. Peptide 238-248 (magenta) within domain MG3 (blue) of C3b has been found to become less exposed to HD exchange after binding of Efb-C. Though Lys-242 (magenta spheres), which is located in the middle of a loop formed by this peptide, represents a contact residue for the ligand CRIg (orange), the binding of CRIg to C3b was not influenced by Efb-C. As the peptide is surrounded by domains LNK (yellow), MG6 (cyan), MG7 (pink), and MG8 (red), which are likely to experience more pronounced Efb-C-induced allosteric changes, its solvent accessibility may be influenced by these neighboring domains rather than direct allosteric effects. The figure shows the C3b-CRIg complex as solvent accessible surface (left) and cartoon representation (right). It was generated from PDB 2ICF (24) using PyMOL.

Allosteric Inhibition of Complement Function by a Staphylococcal Immune Evasion Protein

Figure S10

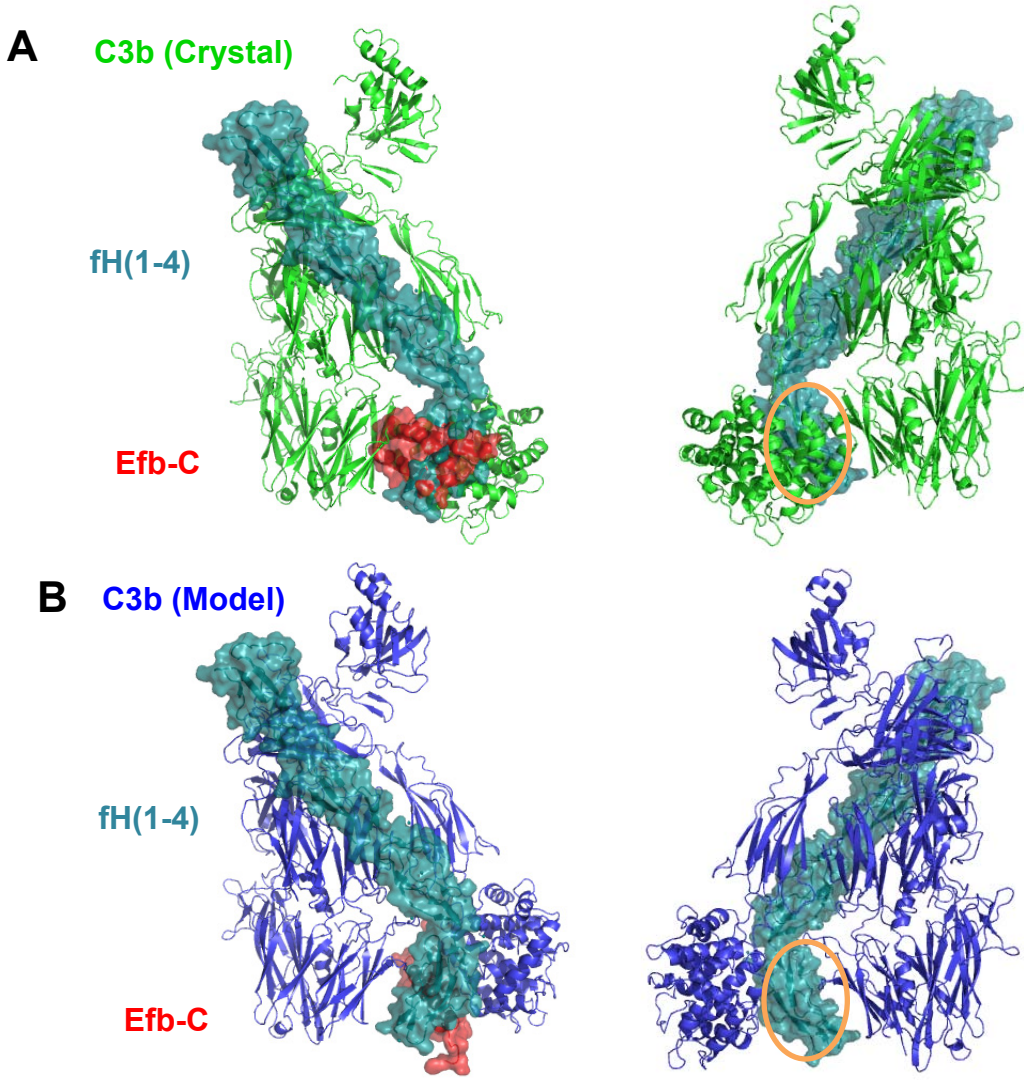

Figure S10. Overlap of binding sites for fH(1-4) and Efb-C on C3b. (**A)** The contact area of fH (cyan) on TED of C3b (green) overlaps with binding site of Efb-C (red), leading to a potential steric clash. (**B)** In the SAXS-derived model (blue), Efb-C dislocates TED-CUB from the remainder of the C3b core and thereby likely disrupts the contact interface on CCP4 of fH (orange circle). In addition, these changes propagate into the MG6-8 region, so that even more contact areas of fH (1-4) may be affected by binding of Efb-C. The figure was generated by superimposing PDB 2WII (25) with PDB 2GOX (**A**; Ref. 9) or the SAXS-BILBOMD model (**B**) using PyMOL.

Figure S11

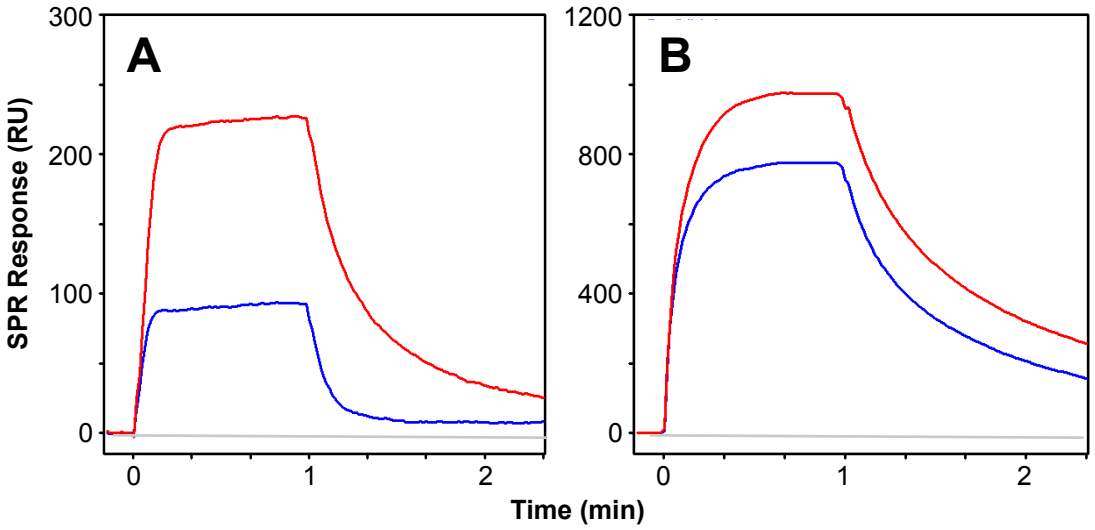

Figure S11. Effect of Efb-C on the binding of fH and its fH(19-20) fragment to C3b. In addition to the fH(1-4) fragment that was evaluated for the HDX-MS and binding site analyses (**Fig. 3**), full-length fH (**B**; isolated from plasma) and its C-terminal fragment fH(19-20) (**A**; recombinantly expressed) was tested at a concentration of 1 µM using the same SPR method. In contrast to fH (1-4), the binding of which to C3b was completely blocked in the presence of Efb-C, both fH and fH(19-20) showed significantly increased binding affinity to the C3b/Efb-C complex (red) when compared to C3b alone (blue). The smaller increase in the case of fH indicates that the observed overall effect of Efb-C on fH binding is a consequence of the two opposite contributions on the two binding areas for C3b, i.e. inhibition of fH(1-4) and potentiation of fH(19-20). The functional consequences of this combinatory effect are not yet clear and have to be further elucidated.

Figure S12

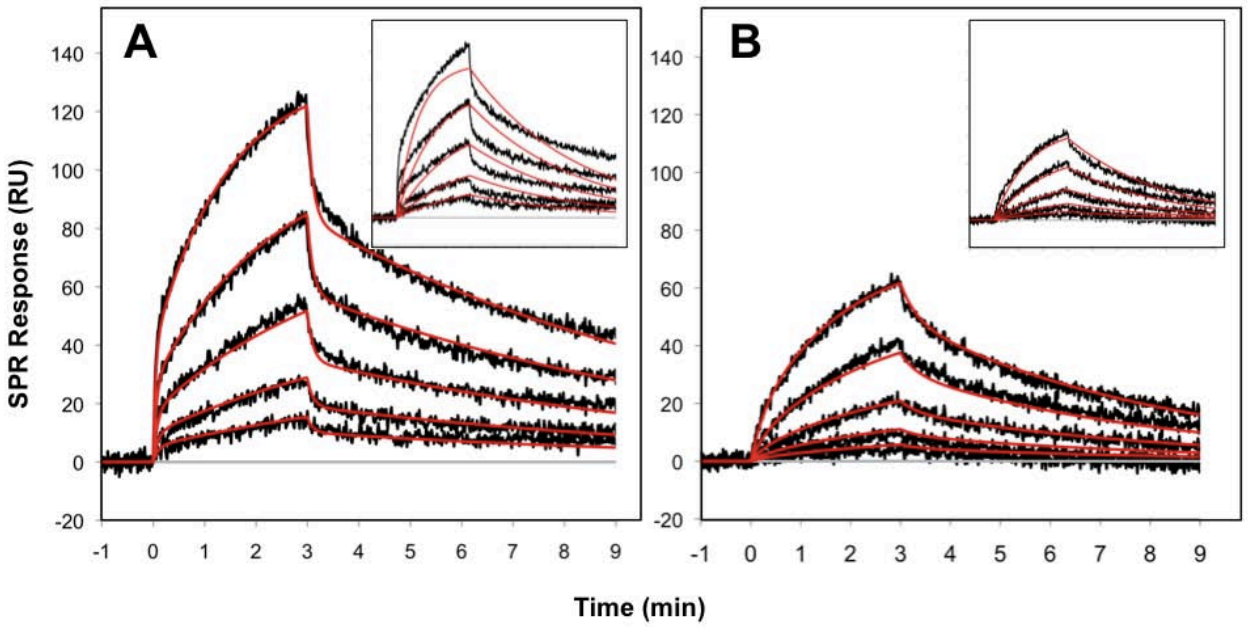

C

	k_{a1} (10^4 $M^{-1}s^{-1}$)	k_{d1} (10^{-2} s^{-1})	K_{D1} (µM)	k_{a2} (10^3 $M^{-1}s^{-1}$)	k_{d2} (10^{-3} s^{-1})	K_{D2} (µM)
C3b	21.3	15.5	0.7	9.9	2.0	0.2
C3b/Efb-C	1.6	5.1	3.2	6.1	3.1	0.5

Figure S12. Kinetic evaluation of the C3b-fB interaction in absence and presence of Efb-C. SPR binding data was acquired on a ProteOn XPR36 biosensor (Bio-Rad) at 25ºC and a flow rate of 25 µM in 10 mM HEPES pH 7.4, 150 mM NaCl, 1 mM $MgCl_2$, 0.005% Tween 20. Biotinylated C3b was captured on a neutravidin-coated sensor chip (NLC; Bio-Rad) and fB was passed over as a 1:1 dilution series (63-1000 nM) (**A**). A C3b/Efb-C complex was formed by injecting 200 nM Efb-C on the C3b channel and the fB injection was repeated (**B**). Interspots and a blank channel were subtracted, and the data sets (black) were fitted to a 'ligand heterogeneity' model[1] (red) using ProteOn Manager v2.1.1 (**C**). Though fB still binds to C3b in the presence of Efb-C, the initial fast event is largely affected in the kinetic association ($k_{a1;}$ highlighted in red) and to some extent in the dissociation rate (k_{d1}), whereas the second slower event experiences a comparatively minor impact (k_{a2}, k_{d2}). In fact, the binding is almost reduced to a 1:1 model in presence (**B**) but not in absence (**A**) of Efb-C (**inserts**). It is believed that the initial binding event is essential for a proper loading of fB to C3b that allows subsequent convertase formation. Despite the similarities in the second binding event, it has to be further investigated whether the residual fB-C3b/Efb-C complex corresponds to the fB-C3b interaction or follows a slightly different binding mode.

[1] It has to be noted that the C3b-fB interaction follows equally well a heterogeneity (two independent binding events) and conformational change model (two connected events), as reported in Ref. 7, and there are observations in support of conformational changes involved in the interaction (7, 34). However, a heterogenity model was chosen in this case to better visualize the differential effect of Efb-C on the two binding events.